Regular and chaotic motion of classical electrons in the wake potential of fast ions in solids

Jörg Müller and Joachim Burgdörfer
Department of Physics, University of Tennessee, Knoxville, Tennessee 37996-1200
and Oak Ridge National Laboratory, Oak Ridge, Tennessee 37831-6377
(Received 31 October 1989)

The classical dynamics of an electron under the influence of a screened Coulomb potential around fast ions in solids is investigated. A transition from regular to chaotic motion as a function of the binding energy is observed. We discuss possible signatures of chaotic dynamics in the final-state distribution of foil-excited atoms.

I. INTRODUCTION

The interaction of fast charged particles with an electron gas causes a coherent electron displacement. This picture of a strongly anistropic distribution of the dynamical screening charge dates back to Bohr,[1] who referred to this phenomenon as "wake" behind the charged particle. An explicit expression for the wake was first given by Neufeld and Ritchie.[2] The "wake" shows a series of domains with alternately enhanced and depleted electron density relative to the mean density of the medium. Accordingly, the electrostatic potential ("wake potential") exhibits in addition to a monotonic decay as a function of distance an oscillatory feature: domains of enhancement create regions of negative electric potential, whereas density depletion gives rise to a positive potential. Dynamical screening around fast particles with velocities v_P larger than the Fermi velocity v_F, the characteristic speed of the electron gases, is different from the isotropic (Debye-type) screening in the static limit ($v_P \rightarrow 0$). Several experimental studies concerning the transmission of fast ions through matter (usually thin foils) have found indications for the existence of the wake potential. They include modifications of the Coulomb explosion after molecular breakup in solids[3] and oscillatory structures in the secondary electron emission.[4] The wake provides a perturbation of the atomic Coulomb field in highly charged ions. For low-lying states ($n \simeq 2$) this perturbation is sufficiently weak as to give rise to a Stark effect that has been observed in resonant coherent excitation of channeled ions by Datz *et al.*[5] and for ions propagating in random direction by Chetoui *et al.*[6] For higher-lying states the perturbation by the dynamical screening charge is strong such that a perturbational treatment breaks down. One expects therefore the complex dynamics in a nonseparable potential to unfold. The goal of the present paper is the study of the dynamics in this regime.

We focus here on the "diffusion" in energy and angular momentum as a signature of chaotic dynamics. Recent experiments have provided evidence for diffusion in angular momentum[7] and energy[8] of the projectile centered excited states. Good agreement with the experimental l distribution has been found employing classical stochastic dynamics to treat effects of electronic multiple scattering in terms of a sequence of "kicks."[9] Due to the breaking of the spherical symmetry by the wake potential l mixing and l diffusion can occur even in absence of collisions. We therefore determine the quantitative importance of this competing transport mechanism.

Another motivation stems from the observation by Neelavathi, Ritchie, and Brandt[10] that the minima in the oscillatory part of the wake potential can trap charged particles. These potential troughs can therefore give rise to transient electronic bound states of "wake-riding" electrons.[11–14] As of now, evidence for these wake-riding electrons in the forward emission spectrum is inconclusive. In a recent theoretical study[15] we have shown that for positively charged particles the cross section for production of convoy electrons is exceedingly small, while for negatively charged particles such as antiprotons ($\bar{p}$) the cross section is much bigger ($\simeq 10^{-22}$ cm^2). This fact, in addition to the suppression of forward scattering of directly ionized electrons by $\bar{p}$, makes their observation more feasible for antiprotons than for protons (or positive ions), if at all possible. First experimental tests[16] using antiprotons from the LEAR facility at Centre Européenne pour la Recherche Nucléaire (CERN) appear to be more promising but not yet conclusive. A better understanding of the transport behavior of wake-riding electrons is therefore desirable.

We investigate the classical motion in both the perturbed Coulomb well and in the first, and most important, trough of the wake in the proximity of the fast ($v_P \gg 1$), highly charged ($Q \gg 1$) ions penetrating a foil. The effects of additional minima at larger distances as well as quantum tunneling between them will be neglected. The classical motion associated with bound states is therefore confined to two disconnected energy shells at negative energies is $E < 0$. At threshold $E = 0$ the two energy shells merge and the classical motion corresponds to irregular scattering in a complicated potential distribution.[17] An analysis of the quantum dynamics in the wake potential is presently underway.[18] Atomic units will be used unless otherwise stated.

II. WAKE POTENTIAL

The following scenario underlies our calculation: A fast highly charged ion penetrates a thin polycrystalline

Al foil. We assume that an electron propagates in close phase-space correlation along with the ion. The source can be either projectile excitation or ionization, i.e., loss of an electron carried into the collision or picked up in an earlier stage of the transmission, or direct capture of a target electron. Since these primary processes occur at high velocities with rather small cross sections, the simultaneous presence of a second electron is statistically unlikely leaving aside here correlated two-electron processes important at lower speeds. We therefore are left with a one-electron problem in a complicated potential generated by the dielectric response of the medium. The medium is assumed to be a homogeneous electron gas. The electrons which are responsible for the response are well separated in phase space such that quantum-mechanical exchange effects are unimportant.

The "active" electron is, in addition to the Coulomb potential V_0, subject to a dynamical screening potential V_1 produced by the displaced electron density. The total potential $V=V_0+V_1$ will be called wake potential.

In linear-response theory[19] the electron density n_s is given by

$$n_s=F(k,\omega)V_0 \ , \tag{1}$$

where $F(k,\omega)$ is the density response function, k the wave number, and ω the frequency. Validity of linear-response theory requires that the induced density fluctuation is small compared to the average density. In the limit of strong perturbation $Q/v_P>1$ this condition is violated. In some of our applications we will choose for illustrative purposes parameters in accordance with experiments by Betz *et al.*,[20] $Q=16$, $v_P=12.5$ a.u. for which this criterion is not met. The potential distribution therefore cannot be expected to be accurate.[21] We note, however, that our analysis of the chaotic phase space is structurally unaffected by this shortcoming. As will be discussed in Sec. III the existence of classical scaling invariances implies that an isomorphic phase-space structure can be found in terms of rescaled variables for different parameter values Q/v_P, in particular, those for which the linearity criterion $Q/v_P<1$ is satisfied.

The response function $F(k,\omega)$ can be expressed in terms of the electric susceptibility $\chi_e(k,\omega)$,

$$F(k,\omega)=\frac{k^2}{4\pi}\frac{-\chi_e}{1+\chi_e} \ .$$

Using Poission's equation we obtain an expression for the dynamical screening potential

$$V_1=\frac{4\pi}{k^2}F(k,\omega)V_0 \ . \tag{2}$$

This leads to the total potential

$$V=\frac{1}{\varepsilon(k,\omega)}V_0 \ , \tag{3}$$

where $\varepsilon(k,\omega)=1-[4\pi F(k,\omega)/k^2+4\pi F(k,\omega)]$ is the dielectric function.

The Fourier transform of the potential of the charge Q moving at the speed v_P is given by

$$V_0=Q\frac{\delta(\omega-kv_P)}{2\pi k^2} \ . \tag{4}$$

Inverse Fourier transformation leads to the following integral expression for the potential in cylindrical coordinates in the frame of the projectile:[2,22]

$$V(z,\rho)=\frac{Q}{\pi v_P}\int_{-\infty}^{\infty}d\omega\int_0^{\infty}d\kappa\frac{J_0(\rho\kappa)\exp(-i\omega z/v_P)}{(\kappa^2+\omega^2/v_P^2)\varepsilon(k,\omega)} \ . \tag{5}$$

The potential is time independent due to our assumption of homogeneity. Here, z is the coordinate in the direction of motion of the projectile, ρ is the distance from the axis, J_0 is the zeroth-order Bessel function, v_P the speed of the projectile in the laboratory frame, and $\kappa=[k^2-(\omega^2/v_P^2)]^{1/2}$. Time-dependent perturbations correspond to scattering processes at inhomogeneities which have been treated elsewhere[9,21] and which we will neglect in the following. Equation (3) describes a nonseparable potential in two degrees of freedom. The aximuthal angle φ is cyclic and l_z is a constant motion due to the rotational symmetry about the $\hat{v}_P$ axis. The potential resembles the one for the well-known example of chaotic motion, the hydrogen is a strong magnetic field. There are, however, two important differences. First, the potential (5) is not invariant under parity transformation ($z\rightarrow -z$) and, second $V(z,\rho)$ is a transcendental (or algebraic) function in the canonical coordinates such that mechanical similarity transformations are not easily applicable (see Sec. III).

The only nontrivial quantity in (5) is the dielectric function $\varepsilon(k,\omega)$ for which an appropriate approximation has to be implemented. Several approximations have been discussed. They include the plasmon-pole approximation with and without dispersion and single-particle effects,[22] the random-phase approximation[23] and variants of it,[23] and mode-coupling approximations.[24] We restrict ourselves in the following to the single plasmon-pole approximation, i.e.,

$$\varepsilon(k,\omega)=\begin{cases}1-\dfrac{\omega_p^2}{\omega(\omega+i\gamma)} & \text{if } k<\dfrac{\omega_p}{v_F}\\ 1 \ \text{ if } k>\dfrac{\omega_p}{v_F} \ ,\end{cases} \tag{6}$$

where ω_p is the plasmon frequency and γ is an empirical damping constant (Drude damping). While the approximation neglects many subtle effects such as bow waves it still accounts for most of the features of the wake. Considering the complexity of the dynamics to be discussed in the following it appears to be adequate to consider only the simplest form of the full wake potential in spite of these obvious shortcomings.

Using (6) Eq. (5) can be simplified to give

$$V(\rho,z)=Q\left[\frac{1}{R}-\frac{\omega_p}{v_P}S_0(\xi,\eta)+\frac{2\omega_p}{v_P}\sin(\eta)K_0\left[\eta,\frac{v_P}{v_F}\right]\exp\left[\frac{z\gamma}{2v_P}\right]\Theta(-z)\right] \ , \tag{7}$$

where

$$R=(z^2+\rho^2)^{1/2},\quad \eta=\frac{\omega_p z}{v_P},\quad \xi=\frac{\omega_p \rho}{v_P}\ .$$

The term

$$S_0(\xi,\eta)=\int_0^\infty dt\frac{J_0(\eta t)e^{-|\xi|t}}{1+t^2} \tag{8}$$

describes the monotonically decaying screening potential as a function of the distance from the ion. We note that in the limit $\omega_p R/v_P \gg 1$ $S_0(\xi,\eta)$ possesses the following asymptotic form:

$$S_0(\xi,\eta)=\frac{v_P}{\omega_p}\left[\frac{1}{R}-\left[\frac{v_P}{\omega_p}\right]^{1/2}\frac{2}{R^3}P_2(z/R)\right], \tag{9}$$

where P_2 is the second-order Legendre polynomial, i.e., at large distances the S_0 term gives rise to a quadrupole potential. The third term in (7) describes the oscillatory part of the potential which is due to the electron density fluctuations trailing the ion and is given by

$$K_0\left[\eta,\frac{v_P}{v_F}\right]=\int_0^{v_P/v_F} dt\frac{J_0(\eta t)}{1+t^2}\ . \tag{10}$$

In the limit $\omega_p R/v_P \gg 1$ we have found the asymptotic limit of Eq. (10) as

$$K_0\left[\eta,\frac{v_P}{v_F}\right]=\frac{\alpha}{\eta^{1.5}}\sin\left[\frac{v_P}{(3\pi^2 n_s)^{1/3}}\eta+\eta_0\right], \tag{11}$$

where α and η_0 are functions of the parameters ω_p, v_P, and n_s and are determined numerically. Equation (11) deviates from the expression[22] in terms of the modified Bessel function K_0 which is only valid in the simultaneous limit $v_P/v_F\to\infty$.

The wake potential (Fig. 1) features two distinct domains: near the projectile the potential behaves like a screened Coulomb potential, whereas for negative z (behind the projectile) the oscillatory part due to the density oscillations of the electron gas clearly dominates. These oscillations have a wavelength of

$$\lambda_w\approx\frac{2\pi v_P}{\Omega}\ . \tag{12}$$

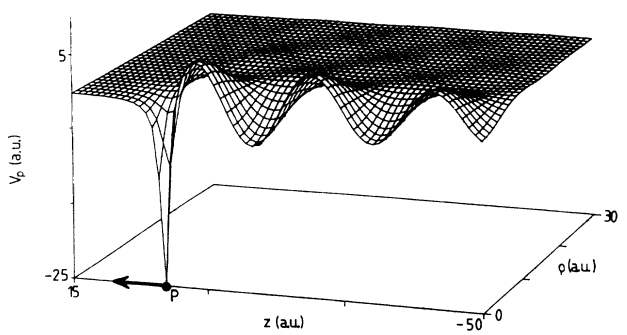

FIG. 1. Dynamical screening potential of S^{16+} in Al calculated in plasmon-pole approximation to the dielectric function ($v_{\rm ion}=1$ a.u.).

In the plasmon-pole approximation the resonance frequency of the medium, Ω, is equal to the plasmon frequency ω_p. The depth of the potential troughs is proportional to the charge Q of the projectile. The wake potential (7) does not include the effect of the self-wake of the electron. Modifications by the self-wake are estimated to be relatively small[25] in the limit $Q\gg 1$.

III. SCALING PROPERTIES

Classical dynamics is governed by the canonical equations of motion which take, in cylindrical coordinates, the form

$$\frac{d\rho}{dt}=p_\rho,\quad \frac{dp_\rho}{dt}=-\frac{dV_{\rm wake}}{d\rho}+\frac{l_z^2}{\rho^3}\ , \tag{13a}$$

$$\frac{dz}{dt}=p_z,\quad \frac{dp_z}{dt}=\frac{dV_{\rm wake}}{dz}\ , \tag{13b}$$

$$\frac{d\varphi}{dt}=\frac{l_z}{\rho^2},\quad \frac{dl_z}{dt}=0\ . \tag{13c}$$

Because l_z is conserved and φ is cyclic Eq. (13) described the motion on the three-dimensional energy hypersurface in the four-dimensional phase space. The energy refers to the energy in the medium. Nonadiabatic effects near the exit surface[23] will be discussed in Sec. V. For reasons of convenience we express the energy of bound electrons in the wake in terms of the n action ("quantum number")

$$E=-\frac{Q^2}{2n^2} \tag{14}$$

which would be the principal action in a pure Coulomb potential. In the wake potential, however, it is only a convenient parametrization for the energy of Rydberg electrons.

Each initial condition is defined in terms of three independent coordinates. In addition, the wake potential is characterized by three additional parameters: v_P, n_s, and γ. Considering the high dimensionality of the parameter space it is tempting to apply mechanical similarity transformations in order to reduce the effective dimensionality of the parameter space. However, the complicated analytic structure of (7) restricts the number of scaling invariances. The only exact scaling transformation we were able to find is ($\beta>0$)

$$\begin{aligned}
&Q\to Q'=\beta Q\ ,\\
&E\to E'=\beta E\ ,\\
&t\to t'=t/\sqrt{\beta}\ ,\\
&n\to n'=\sqrt{\beta}n\ ,\\
&l\to l'=\sqrt{\beta}l\ ,\\
&p_i\to p_i'=\sqrt{\beta}p\ ,\\
&q_i\to q_i'=q_i\ ,
\end{aligned} \tag{15}$$

where l is the total angular momentum of the electron and (p_i,q_i) are the canonical momenta and coordinates.

This transformation involves only atomic (projectile) variables while leaving parameters characterizing the electron gas invariant. Since this transformation does not involve v_P, any value of the linearity parameter for the dielectric response, Q/v_P, can be reached. For later reference we note that all numerical results presented in the following remain unchanged for all values of Q/v_P, apart from appropriately rescaling the variables E, n, l, p_i, and t according to (15).

In addition, we have found an approximate scaling invariance which involves only electron gas (target) parameters and v_P while leaving atomic variables unchanged:

$$\begin{aligned} v_P &\rightarrow v_P' = \beta v_P \ , \\ \gamma &\rightarrow \gamma' = \beta\gamma \ , \\ n_s &\rightarrow n_s' = \beta^2 n_s \ . \end{aligned} \tag{16}$$

This transformation would constitute an exact scaling invariance if one neglects the change in the cutoff $k_c = \omega_p / v_F$ [see Eq. (6)]. Since $k_c'/k_c = \sqrt[3]{\beta}$ changes in the cutoff are small for β values of the order of 1. Equation (16) allows us therefore to approximately relate the dynamical behavior in different media of similar electronic density.

IV. CLASSICAL MOTION IN THE WAKE

A. Trajectories

In order to obtain classical trajectories of an electron in the wake potential we solve the equations of motion numerically. As is the case for other problems displaying a Coulomb-like singularity at the origin, special care has to be taken to avoid numerical instabilities. We use therefore the Kustaanheimo-Stiefel transformation[26] which maps the Coulomb part of the potential V_0 onto two coupled harmonic oscillators. The singularity at the origin is thereby removed at the expense of the increase of the dimension of the problem since the physical time must be transformed to a new "time." This transformation increases the number of differential equations to be solved by 1. The increase in accuracy by employing this transformation should not be overestimated because of the simultaneously occurring singularity in momentum space.

Since the calculation of the force in the wake is time-consuming, its components were tabulated on a grid. For terms containing S_0 [see Eq. (7)] the two-dimensional grid for the domain $0.1 \le R \le 100 a.u.$ consists of 10^5 points. For the terms containing K_0 the one-dimensional grid consists of 2.5×10^4 points covering the range $0 \le \rho \le 400$ a.u. For larger values of the arguments we use the asymptotic forms [Eq. (9) and (11)].

Comparison with experimental data or quantal calculations are meaningful only for ensemble averages over classical trajectories. Initial conditions for an ensemble of given energy, angular momentum, etc. were chosen at random. The study of individual trajectories provides, however, a detailed insight into the dynamics.

We first present some typical trajectories in the wake potential in the perturbed Coulomb well. We display the trajectory using the Cartesian coordinate system in the frame of the projectile. The projectile moves in positive z-direction. The z-component of the angular momentum l_z is 1 for all trajectories, however, the results are qualita-

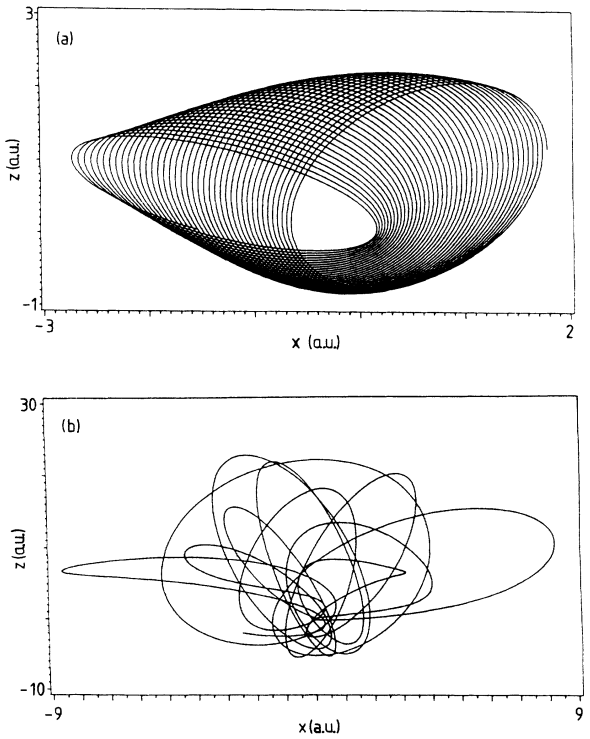

FIG. 2. Trajectory of an electronic orbit in $S^{15+}(v_{ion} = 12.5$ a.u.) in Al with an energy corresponding to an unperturbed state with quantum number (a) $n = 5$ and (b) $n = 25$ state.

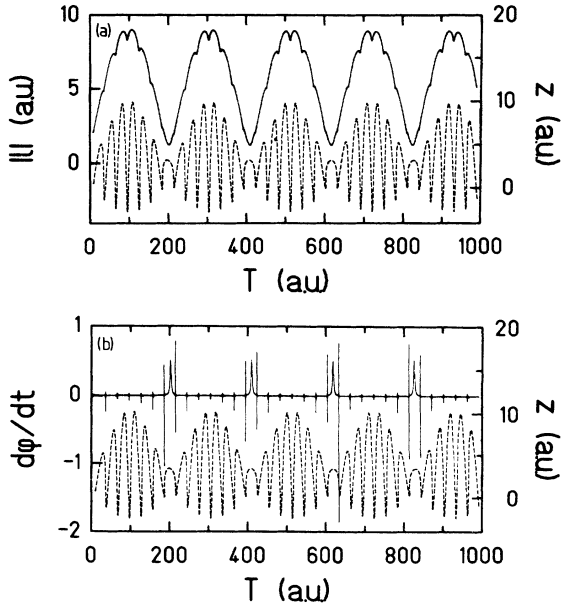

FIG. 3. Time evolution of z (— — —), l (——) (a), and $d\varphi/dt$ (——) (b). Initial conditions: $n = 14$, $l_z = 1$, $z = 0$, $\rho = 2$ a.u., $p_z = 0.866$, $p_\rho = 3.6$.

tively insensitive with respect to the choice of l_z. Figure 2(a) shows the x and z coordinates of a trajectory at $n=5$, which corresponds to a low-lying state with a binding energy of 5.17 a.u. (or ≈ 139 eV). The motion is obviously regular and quasiperiodic. Two features are evident: the ellipse precesses which indicates a deviation from the $1/R$ behavior of the Coulomb potential. In addition, the ellipse changes shapes in a "breathing" mode. The latter corresponds to a change of its eccentricity, or of the angular momentum of the orbit. This is nothing but the classical manifestation of the Stark effect. For low-lying states well localized around the nucleus the (distant) displacement of electron density trailing the ion produces an effective electric field which leads to quasiperiodic fluctuations in the angular momentum. Chetoui *et al.*[6] have recently reported on the observation of such fluctuations in hydrogenic krypton ($n=2$) traversing carbon foils at $v_P=36$ a.u. For higher n most trajectories become manifestly chaotic, an example of which is shown in Fig. 2(b) for an $n=25$ orbit.

The mechanism by which chaotic dynamics comes about can be most easily identified by simultaneously following the z coordinate and another dynamical variable like the angular momentum and its polar angle [Figs. 3(a) and 3(b)]. For a trajectory which is still regular but corresponds to a highly excited state ($n=10$) we observe in addition to regular oscillations sharp structures, i.e., "edges" in the curve exactly at those times when z is at its minimum. At those times we also have fast changes in the polar angle of the angular momentum [see Fig. 3(b)]. This is due to a "collision" at the first hump of the wake (see Fig. 1). It appears that the electron gets a "kick" each time it approaches this hump. In Fig. 3(a) we see that the envelope of the oscillations in z direction has the same period as the oscillation of the angular momentum. This is the period of the precession of the trajectory around the projectile. On the other hand, we observe the period of the orbit around the projectile, which appears in the oscillations in z direction. Accordingly, we have two frequencies for this trajectory which are closely related to the motion on a torus. If now the periodic kicks due to the hump in the wake perturb the system the tori start to break up, in particular, for rational winding numbers of the two frequencies.[18] We have found approximate phenomenological formulas for the two fundamental periods. The period τ_1 of one revolution around the projectile is given by

$$\tau_1 \approx 2\pi \frac{n^3}{Q^2} \quad \text{if } n < 1.5\sqrt{Q} \ , \tag{17a}$$

$$\tau_1 \approx 3\pi \frac{n^2}{Q^{1.5}} \quad \text{if } n > 1.5\sqrt{Q} \ . \tag{17b}$$

Equation (17a) closely resembles the pure Coulomb case because the screening effcts are small near the projectile. The period τ_2 of the precession, which is also the period we observed for the change in the absolute value of the angular momentum, is given by

$$\tau_2 \approx \frac{232}{Qn^3}(n-2.5\sqrt{Q})^4 + \frac{800}{\sqrt{Q}} \ . \tag{18}$$

In the limit of small n the Runge-Lenz vector will be a conserved quantity, i.e., the precession period $\tau_2 \to \infty$. The limit $\tau_1/\tau_2 \to \infty$ corresponds to the perturbational regime where destabilizing low-order resonances are suppressed.

A qualitatively similar behavior is observed for trajectories confined to the first wake trough behind the Coulomb well (Fig. 4). In the low-energy case $n=8$ we obtain "Lissajous figures" [Fig. 4(a)] which are typical for coupled harmonic oscillators with different oscillator frequencies. That is due to the fact that the harmonic oscillator is a relatively good approximation near the bottom of the wake well. This approximation breaks down for higher energies. For energies near threshold, $n \approx 1000$, we find within the chaotic regime an intermittent behavior [Fig. 4(b)]. Most of the time the electron oscillates mainly in z direction, whereas the amplitude in ρ direction remains small. Sometimes, however, the trajectory breaks out and explores regions of phase spaces with a larger ρ coordinate. After a short time interval the electron returns to the region with small ρ. The continuation of this behavior across threshold leads to irregular scattering.[17] Trajectories above threshold tend to stay in the region of small ρ bouncing back and forth between the two humps for a long time. Unlike trajectories with negative energies, they escape as soon as they explore regions of large ρ.

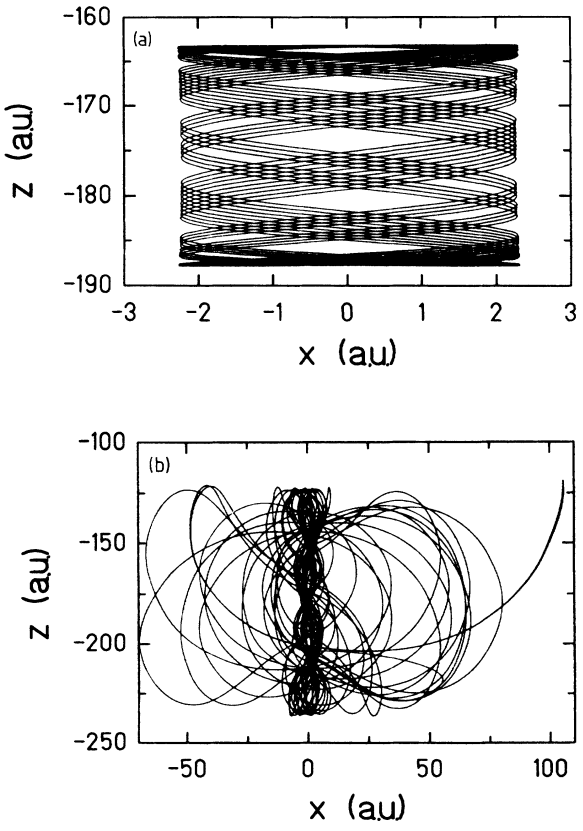

FIG. 4. Orbit of an electron in the first wake trough behind the projectile; (a) $n=8$, $l_z=0$, and (b) $n=1000$, $l_z=1$.

B. Poincaré maps

Poincaré maps are defined as intersections of the trajectory with a given plane in phase space.[27,28] The dynamics is confined in the present case to a three-dimensional energy hypersurface. We have chosen z, ρ, and p_ρ (the momentum in ρ direction) as independent coordinates and the plane $z=$const. Since every trajectory has two intersections per revolution with the plane $z=$const, we define the Poincaré map in terms of the intersection with positive $p_z>0$. Figures 5(a)–5(c) are Poincaré maps for trajectories near the ion where the Coulomb part of the wake is dominant. We have chosen an n (or energy) dependent plane $z=n/10$ as the surface of section. This is because of the singularity in the Coulomb potential which causes the momenta to diverge in the limit of small distances (which implies small z). If we choose the z too large, we would miss some trajectories, especially for small n. As initial coordinates we chose z on the surface of section. We vary the launching angle relative to the z axis from 0 to $(2\pi-2\pi/m)$ in steps of $2\pi/m$ if we use m trajectories.

For regular trajectories the electron moves on tori in phase space (Kolmogorov-Arnold-Moser tori).[27,28] The intersection of these tori with the Poincaré plane results in closed curves on the map. This implies that one can find another constant of motion (action variable) for these trajectories beside the energy and the z component of the angular momentum. In the case of higher n we observe regions in phase space with scattered points [Fig. 5(b)]. This means that the motion of the electrons is no longer confined to tori, or in other words, there is no additional constant of motion (besides energy and l_z). The chaotic

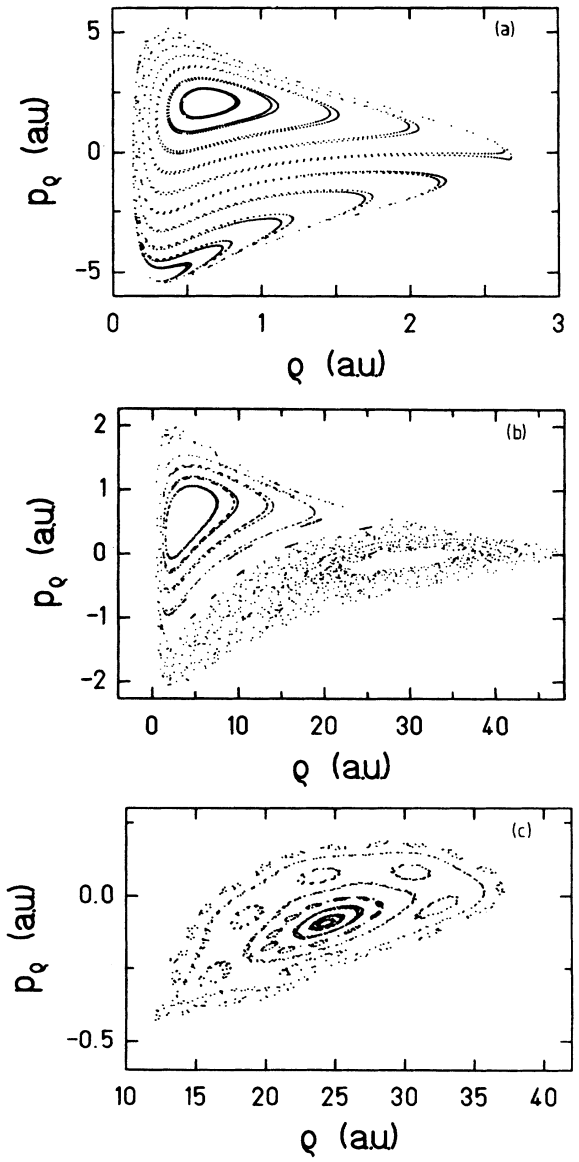

FIG. 5. Poincaré surface of section ($\rho-p_\rho$ plane) for the motion near the projectile. Initial conditions (a) $n=5$, $l_z=1$, $1\le l_i\le 3.6$; (b) $n=60$, $l_z=1$, $1\le l_i\le 12.3$; (c) magnification of (b).

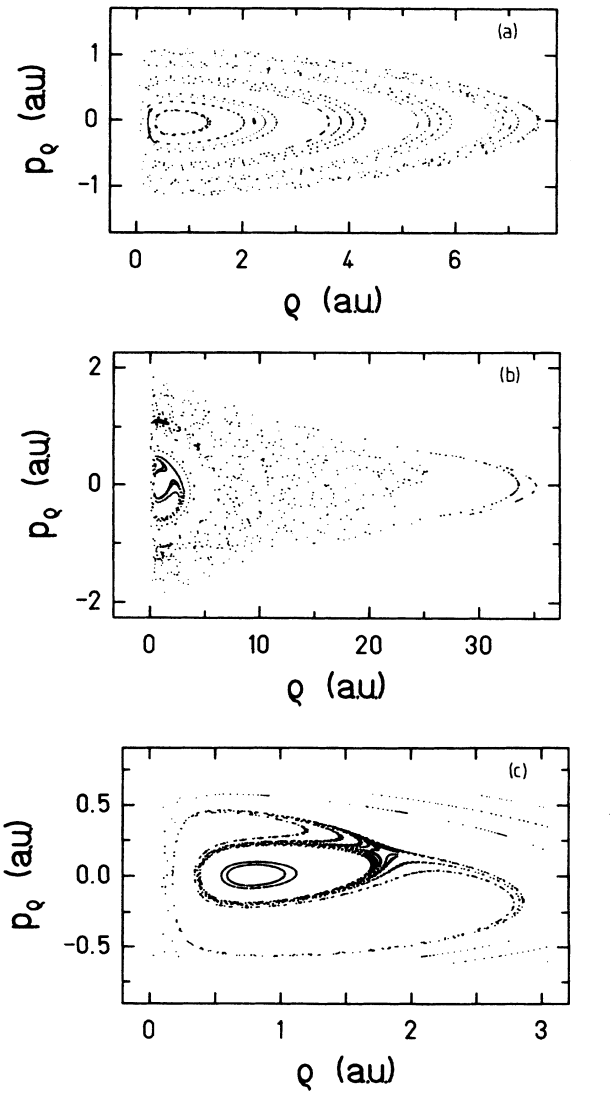

FIG. 6. Poincaré surface of section ($\rho-p_\rho$ plane) for the motion in the first trough of the wake (a) $n=10$, $l_z=1$, (b) $n=20$, $l_z=1$; (c) magnification of (b).

regime is mainly situated in the lower part of the map. This refers to trajectories which have their apocenter at negative z values. Those trajectories are more strongly influenced by the first potential maximum than those with apocenters at positive z values and therefore tend to show a more pronounced chaotic behavior. This observation confirms our previous findings that the interaction with the humps causes the motion to become irregular. The breakup of tori and the formation of island chains can be observed in Fig. 5(c) which is a magnification of the regular region in Fig. 5(b). According to the Poincaré-Birkhoff theorem, the island chains consist of alternating hyperbolic and elliptic fixed points. Around an elliptic point we find stable rotational motion, whereas near the hyperbolic points the motion becomes unstable and almost all orbits are driven away from it.

Similar results are observed for the Poincaré maps for the motion in the wake minimum [Figs. 6(a)–6(c)]. The plane in phase space is z = -175.34 a.u. The initial conditions in coordinate space are ($z=-175.34$, $\rho=2.1$), which is close to the minimum of effective potential V_{eff}

$$V_{\text{eff}}(z,\rho)=V_{\text{wake}}(z,\rho)+\frac{l_z^2}{\rho^2} , \tag{19}$$

with $l_z=1$. The launching angles relative to the z axis are varied between 0 to $2\pi-2\pi/m$ in steps of $2\pi/m$ if we use m trajectories. It has been checked that in the limit of large m we cover the whole hypersurface at a given energy.

As expected the motion becomes mostly chaotic near the ionization threshold. However, there are still regions with closed curves, i.e., regular motion: the first one near the origin (ρ and p_ρ are small), in this case the electron oscillates mainly in z direction; and a second one "at the border" (ρ and p_ρ big), which indicates that the amplitude of the oscillation is large in the ρ direction, whereas the amplitude in z direction remains small. This feature is easy to understand. In each of these extreme cases one of the two degrees of freedom is "frozen out" rendering the system one dimensional and therefore regular.

C. Lyapunov exponents

For the quantitative description of chaotic motion we use local Lyapunov exponents $\lambda(x_0)$ and ensemble-averaged Lyapunov exponents $\langle\lambda\rangle$. The Lyapunov exponents describe "how fast" two initial conditions near x_0 separate in phase space as a function of time,

$$\lambda(x_0)=\lim_{T\to\infty}\lim_{\varepsilon\to 0}\frac{1}{T}\ln\left[\frac{\|f(x_0)-f(x_0+\varepsilon)\|}{\|\varepsilon\|}\right] . \tag{20}$$

The number of Lyapunov exponents equals the dimension of the Poincaré map. According to Liouville's theorem, at most half of these can be positive, the largest of which is called the maximum Lyapunov exponent $\lambda_{\max}$. In the present case of a two-dimensional mapping there is only one positive Lyapunov exponent, which coincides with $\lambda_{\max}$ and will be denoted by λ. $\lambda>0$ implies exponential separation, i.e., chaotic motion, while $\lambda=0$ indicates regular motion.

In order to obtain λ we used a method proposed by Froeschle[29,30] and Benettin, Galgani, and Strecyn.[31] We consider the Poincaré surface of section of the trajectory x (initial condition x_0) and of a set of trajectories ξ_1, $\xi_2,\ldots,\xi_n$ where n is the dimension of the surface of section (in our case, 2). The trajectories ξ_i are defined by initial conditions

$$x_0-\xi_i(0)=\varepsilon_i e_i , \tag{21}$$

where $\xi(0)$ is a point on the surface of section, ε_i is a small number, and e_i is a unit vector in the ith coordinate of the Poincaré map. $\xi(k)$ is the kth intersection of $x(k)$ with the surface and $\xi_i(k)$ the kth intersection of ξ_i. We calculate the stability matrix $M(0,k)$, which is defined as

$$M_{i,j}(0,k)=\frac{x(k)-\xi_j(k)}{x_0-\xi_i(0)} . \tag{22}$$

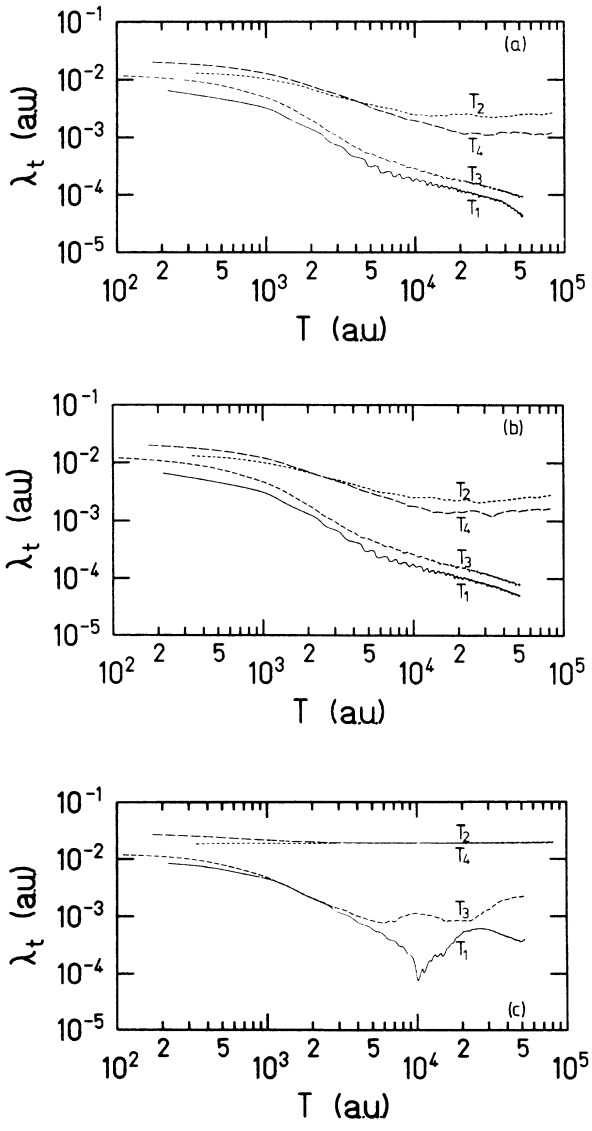

FIG. 7. Dependence of $\lambda(t_k)$ on the distance between initial conditions, $\varepsilon=\sum|\varepsilon_i|$, for four different trajectories T_{1-4} (see text). (a) $\varepsilon=3\times10^{-4}$; (b) $\varepsilon=3\times10^{-5}$; (c) $\varepsilon=1\times10^{-7}$.

We define the function

$$\lambda(t_k)=\frac{1}{t_k}\ln\|M(0,k)\| \ , \tag{23}$$

where the t_k refers to points in time when the trajectory x intersects with the Poincaré map. The Lyapunov exponent is defined as the limit

$$\lim_{\sum|\varepsilon_i|\to 0}\lim_{k\to\infty}\lambda(t_k)=\lambda(x_0) \ . \tag{24}$$

Since it is numerically not practical to reach these limits, we make k sufficiently large such that the function $\lambda(t)$ is nearly constant for times larger than t_k and the ε_i must not be chosen too small in view of numerical roundoff errors.

In Figs. 7(a)–7(c) we show the dependence of $\lambda(t_k)$ on ε_i. We chose four trajectories all at an energy of -0.32 a.u. which corresponds to $n=20$ in the wake trough. Two of those trajectories (T_1 and T_3) are regular. An electron which moves along T_3 oscillates mainly in z direction, whereas an electron on T_1 oscillates mainly along the ρ direction. The other two trajectories (T_2 and T_4) are chaotic.

For regular trajectories $\lambda(t_k)$ should converge to zero, whereas for chaotic trajectories $\lambda(t_k)$ should converge to a constant positive value. This behavior cannot be expected to be exactly observable in the numerical study. What we can expect is that for regular trajectories $\lambda(t_k)$ will decrease and will finally be less than a critical value, whereas for chaotic trajectories $\lambda(t_k)$ will fluctuate around a constant value which will be identified as a Lyapunov exponent. This value should be above the critical value, otherwise λ is set to be zero. Numerical noise poses a major problem in accurately determining λ. This is illustrated in Figs. 7(a)–7(c) where $\varepsilon=\sum|\varepsilon_i|$ (in scaled variables) takes the values 3×10^{-4}, 3×10^{-5}, and $1\times10.^{-7}$ While $\lambda(t_k)$ is structurally stable as ε is reduced by a factor of 10 [Fig. 7(b)] noise dominates the evolution for regular trajectories leading to λ values above the critical value if ε is made even smaller [Fig. 7(c)].

The chaotic dynamics for an energy shell or an ensemble of shells can be described by average Lyapunov exponents $\langle\lambda\rangle$ determined by an average over a set of initial conditions for a given ensemble chosen at random.

Figure 8 shows $\langle\lambda\rangle$ as a function of energy for the energy shell pertaining to the first wake minimum. For small energies, i.e., small n, the Lyapunov exponent is zero [all calculated $\lambda(t_k)$ are finally less than the critical value], indicating that all trajectories are regular. With increasing energy (increasing n), $\langle\lambda\rangle$ becomes positive. We observe a rather sharp (phase-transition-like) onset of chaotic motion near $n=12$ followed by a transition to a predominately chaotic phase space. In this transition regime fluctuations in $\langle\lambda\rangle$ can be observed. For $n>60$ the Lyapunov exponent remains nearly constant because for those energies most of the phase space is chaotic and the Lyapunov exponent of individual trajectories in this chaotic region does not depend strongly on the energy.

The averaged Lyapunov exponents for energy shells pertaining to the Coulomb well are presented in Fig. 9. The first chaotic regions in phase space appear for $n>20$ (energies greater than -0.32 a.u.), which is much higher than in the first minimum of the wake. It appears that the strong Coulomb force suppresses chaotic behavior. It should be noted that $\langle\lambda\rangle$ was calculated only for $n=5,10,20,30,\ldots,100$ since the calculations are rather time-consuming. The resolution of $\langle\lambda\rangle$ is therefore insufficient to analyze any detailed structures in the n dependence of $\langle\lambda\rangle$.

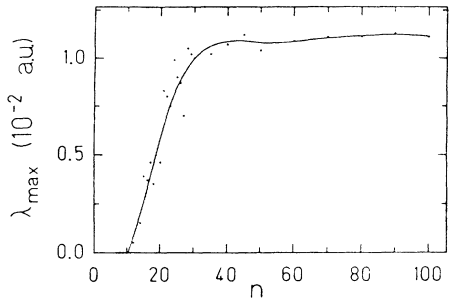

FIG. 8. Averaged Lyapunov exponent as a function of n in the first trough of the wake. Each ensemble consists of 40 randomly distributed initial conditions. The solid curve interpolates between data points.

In view of our study of the angular momentum diffusion we also have investigated the dependence of $\langle\lambda\rangle$ on the angular momentum of the initial orbit in the perturbed Coulomb well (Fig. 10). At a given energy n and l_z the absolute value of l in our simulation ranges from l_z to l_{max} which is for $v_p/\sqrt{n_s}=133$ (i.e., $v_P=12.5$ a.u. in Al) approximately given by the empirical formula

$$l_{max}(n)\approx n[1-(1+92n^{-1.31})^{-1}] \tag{25}$$

and which we have found to be adequate for $n\lesssim 80$. The fact that $l_{max}\ll n$ for high n is due to the screening by the electron gas. For $n=70$, Eq. (22) predicts $l_{max}(n=70)\simeq 18$. We have performed this calculation only for one energy of -0.07 a.u. ($n=70$) because the accumulation of sufficient statistics is very time-consuming. The results are, however, expected to be independent of n for $n\gtrsim 40$. Trajectories with a low initial angular momentum have a higher tendency to show chaotic motion than those with higher initial angular momentum.

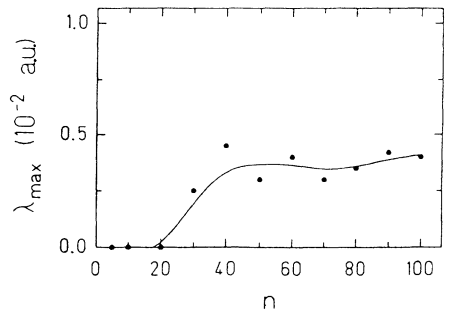

FIG. 9. As Fig. 8 but for trajectories in the Coulomb well.

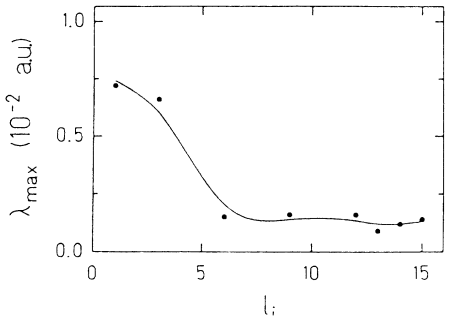

FIG. 10. Averaged Lyapunov exponent for trajectories in the Coulomb well as a function of l_i ($n=70$), l_z is uniformly distributed in the interval $0 \le l_z \le l_i$. Each ensemble consists of 40 randomly distributed initial conditions.

Orbits with low angular momentum have a larger maximum distance from the ion and are therefore more affected by the first hump of the wake oscillations behind the ion.

V. ANGULAR MOMENTUM DIFFUSION

In the following we study the diffusion of angular momentum due to the intrinsic stochasticity of the evolution in the wake field. Our calculation refers to the following scenario: A hydrogenic projectile in initial state (n_i,l_i) enters the solid. The transition from the pure Coulomb potential outside the foil to the wake potential inside is treated in sudden approximation,[32] i.e., the electrons undergo a nonadiabatic transition due to the sudden onset of screening from the well-defined energy shell pertaining to n_i to an energy shell, n, inside the foil determined by the wake potential. For an ensemble of initial orbits of given (n_i,l_i) this leads to a distribution in n. For $v_P=12.5$ a.u. in aluminum and $n_i \le 15$ we found the following empirical relation between the expectation value $\langle n \rangle$ of this distribution and n_i:

$$\langle n \rangle \approx \left[n_i^{-2} - \frac{0.0685}{Q} \right]^{-0.5} . \tag{26}$$

After traversing the solid, a thin foil of thickness d, in the dwell time $T(d)$ the electron undergoes another sudden transition to final states $(n_f l_f)$ in the Coulomb field. The final-state angular momentum distribution l_f as a function of the initial quantum number $(n_i l_i)$ is an indication of the intrinsically stochastic evolution inside the foil.

This scenario is a strongly simplified model for two recent experiments: the double-foil experiments by Betz *et al.*,[20] where the first foil creates the state $(n_i l_i)$ and the second foil perturbs this state and for the proposed high-charge state, high-energy experiment by Rozet *et al.* at GANIL (Ref. 33), where the excited state is producing near the entrance surface in an adsorbed layer of high-Z material while the low-Z foil material (carbon) has a low capture cross section such that the foil transmission is essentially unperturbed by charge-changing collisions.

In order to contrast the differences in the evolution of the angular momentum distribution in the regular and chaotic regimes we display in Figs. 11(a) and 11(b) the distribution parameters $\langle l_f \rangle$ and $\sigma(l_f)$ for $n_i=13$ and 15. In both cases we chose $l_i=2$. Each ensemble is comprised of 100 randomly chosen trajectories. For $n_i=13$ (or $\langle n_{\text{wake}} \rangle = 24.7$) the dynamics is most regular. The expectation value $\langle l_f \rangle$ fluctuates strongly but approximately periodically. After a period $\tau \simeq 280$ a.u. the initial value is almost recovered. The standard deviation $\sigma(l_f)$ remains small. These periodic fluctuations are a classical manifestation of the Stark effect. They result from a quasiperiodic motion on tori which implies near recurrence. For $n_i=15$ ($\langle n_{\text{wake}} \rangle = 78.3$) the phase space is largely chaotic. The expectation value $\langle l_f \rangle$ shows a strongly damped oscillation after an initial steep rise and relaxes to a large equilibrium value which is close to $l_i \simeq n_i$. At the same time $\sigma(l_f)$ approaches a large constant value. The intrinsic chaotic dynamics leads therefore to "mixing" in angular momentum i.e., to an approach of an approximately statistical distribution due to a diffusive behavior.

This wake-field induced mixing competes with another mechanism, the multiple scattering inside the solid, which has been previously shown[9] to induce angular momentum diffusion. The final l distribution is therefore a combination of these two very different processes. The present analysis permits a comparison of the quantitative importance of the two mechanisms. The characteristic diffusion time τ_D due to perturbation by the wake field

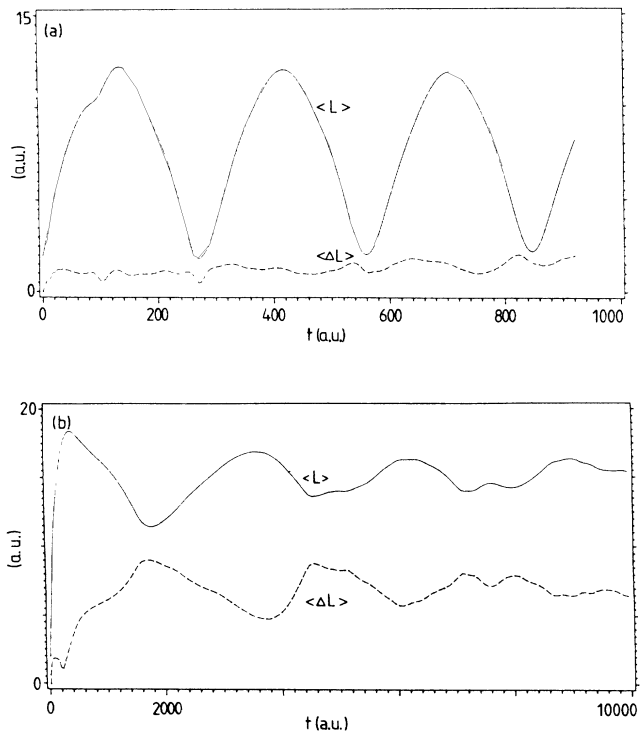

FIG. 11. $\langle l_f \rangle$ and standard deviation $\sigma(l_f)$ as a function of dwell time T. Each ensemble consists of 100 randomly chosen initial conditions with $0.2 \le l_z \le l_i$, $l_i=2$. (a) $n_i=13$; (b) $n_i=15$.

can be estimated from

$$\langle l_f(\tau_D)\rangle \simeq \langle l_f\rangle_{\rm eq}/2 ,$$

where $\langle l_f\rangle_{\rm eq}$ is the approximate equilibrium value of l_f, to be $\tau_D \simeq 100$ a.u. (see Fig. 11). τ_D is large compared to the characteristic collision time $t_c \simeq \lambda_{\rm MFP}/v_P$, $\simeq 5$ a.u., where $\lambda_{\rm MFP}$ is the mean free path for a quasi-free Rydberg electron scattering. This confirms the interpretation of experimentally observed l distribution[7] in terms of multiple scattering effects. For quasifree electrons with orbital diameters exceeding the lattice spacing transitions due to multiple scattering with ionic cores dominate over wake-field induced diffusion. For low-lying states, however, the effective mean free paths, and hence, τ_c, increased rapidly $\propto n^{-4}$. The diffusion time, τ_D scales approximately as $\propto n^{-2}$ as estimated from the Stark effect. Therefore τ_D can become comparable to τ_c so that perturbation of the l distribution by the wake potential investigated in this paper can become important for low to intermediate n.

VI. CONCLUDING REMARKS

We have observed a sharp transition from regular to chaotic motion as a function of the energy (or n) of the electron in the wake potential of fast highly charged ions in a solid. Both perturbed Coulomb orbits near the ion and bound orbits in the first wake troughs possess a divided phase space of regular and chaotic motion. A signature of chaotic motion can be found in the l distribution of excited projectile states. Its quantitative importance depends, however, on the relative strength of the competing perturbation by multiple scattering in the solid. In the case we have investigated so far, collisional redistribution appears to take place on a shorter time scale. The present investigation deals with the classical dynamics of the problem. An investigation of the quantum dynamics of the electronic motion is currently underway.

ACKNOWLEDGMENTS

This work was supported in part by the National Science Foundation and by the U.S. Department of Energy, Office of Basic Energy Science, Division of Chemical Sciences, under Contract No. DE-AC05-840R21400 with Martin Marietta Energy Systems, Inc. One of us (J.M.) acknowledges the support by a Fulbright stipend and by the Studienstiftung des Deutschen Volkes.

[1]N. Bohr, K. Dan Vidensk. Mat.-Fys. Medd. **18**, No. 8 (1948).
[2]J. Neufeld, R. H. Ritchie, Phys. Rev. **98**, 1632 (1955); **99**, 1125 (1955).
[3]D. Gemmell, J. Remillieux, J. Poizat, M. Gaillard, R. Holland, and Z. Vager, Phys. Rev. Lett. **34**, 1420 (1975).
[4]H. Frischkorn, K. O. Groeneveld, P. Koschar, R. Latz, and J. Schader, Phys. Rev. Lett. **49**, 1671 (1982).
[5]S. Datz *et al.*, Phys. Rev. Lett. **40**, 843 (1978); O. Crawford and R. Ritchie, Phys. Rev. A **20**, 1848 (1979).
[6]A. Chetioui, J. Rozet, K. Wohrer, D. Vernhet, A. Touati and C. Stephan, in *Electronic and Atomic Collisions*, edited by H. Gilbody, W. Newell, F. Read, A. Smith (North-Holland, Amsterdam, 1988), p. 309.
[7]Y. Yamazaki *et al.*, Phys. Rev. Lett. **61**, 2913 (1988).
[8]A Mohagheghi *et al.*, *Book of Invited Papers, Proceedings of the Sixteenth International Conference on the Physics of Electronic and Atomic Collisions*, edited by A. Dalgarno (AIP, New York, in press).
[9]J. Burgdörfer and C. Bottcher, Phys. Rev. Lett. **61**, 2917 (1988).
[10]V. N. Neelavathi, R. H. Ritchie, and W. Brandt, Phys. Rev. Lett. **33**, 370 (1974); **33**, 640 (E) (1974).
[11]A. Gladieux and A. Chateau-Thierry, Phys. Rev. Lett. **47**, 786 (1981).
[12]M. Day, Phys. Rev. Lett. **44**, 752 (1980).
[13]Y. Yamazaki and N. Oda, Nucl. Instrum. Methods **194**, 415 (1982).
[14]P. Echenique and R. Ritchie, Phys. Lett. **111A**, 310 (1985); P. Echenique, F. Flores, and R. H. Ritchie, Nucl. Instrum. Methods B **33**, 91 (1988).
[15]J. Burgdörfer, J. Wang, and J. Müller, Phys. Rev. Lett. **62**, 1599 (1989); in Proceedings of the 12th International Conference on Charged Particle Penetration Through Matter, San Sebastian, 1989 (unpublished).
[16]Y. Yamazaki (private communication).
[17]J. Müller and J. Burgdörfer (unpublished).
[18]J. Müller, J. Burgdörfer, and D. Noid (unpublished).
[19]See, e.g., W. A. Harrison, *Solid State Theory* (McGraw-Hill, New York, 1970), p. 280ff.
[20]H. D. Betz, R. Höppler, R. Schramm, and W. Oswald, Nucl. Instrum. Methods B **33**, 185 (1988).
[21]A. Faibis, R. Kaim, I. Plesser, and Z. Vager, Nucl. Instrum. and Methods **170**, 99 (1980).
[22]P.M. Echenique, R. H. Ritchie, and W. Brandt, Phys. Rev. B **20**, 2567 (1979).
[23]A. Mazarro, P. M. Echenique, and R. H. Ritchie, Phys. Rev. B **27**, 4117 (1982); S. Ichimaru, Rev. Mod. Phys. **54**, 1017 (1982).
[24]J. Thakur and K. Pathak (unpublished).
[25]P. Echenique, W. Brandt, and R. H. Ritchie, Phys. Rev. B **33**, 43 (1986).
[26]E. L. Stiefel and G. Scheifele, *Linear and Regular Celestical Mechanics* (Springer-Verlag, New York, 1971), Chaps. 1 and 2.
[27]A. J. Lichtenberg and M. A. Liebermann, *Regular and Stochastical Motion* (Springer-Verlag, Heidelberg, 1982).
[28]H. G. Schuster, *Deterministic Chaos* (VHC-Verlagsgesellschaft, Weinheim, 1988).
[29]C. Froeschle, Astrophys. Space Sci. **14**, 110 (1971).
[30]C. Froeschle and J. -P. Schneider, Astrophys. Space Sci. **25**, 373 (1973); Comput. Phys. **11**, 423 (1973).
[31]G. Benettin, L. Galgani and J. M. Strecyn, Phys. Rev. A **14**, 2338 (1976).
[32]J. Burgdörfer, in *Transport Theory for Convoy Electrons and Rydberg Electrons in Solids*, Vol. 294 of *Lecture Notes in Physics* (Springer-Verlag, Berlin, 1988), p. 344.
[33]J. P. Rozet and A. Chetoui (private communication).